New Astronomy 109 (2024) 102194

Contents lists available at ScienceDirect

New Astronomy

journal homepage: www.elsevier.com/locate/newast

The analysis of type II and type III solar radio bursts: GUI for the e-CALLISTO data

Yashan Hettiarachchi [a,*], Janaka Adassuriya [b], Chandana Jayaratne [b], Sasani Jayawardhana [a], Christian Monstein [c]

[a] University of Sri Jayewardenepura, Nugegoda, Sri Lanka
[b] Astronomy and Space Science Unit, Department of Physics, University of Colombo, Colombo 03, Sri Lanka
[c] Istituto ricerche solari Aldo e Cele Daccò (IRSOL), Università della Svizzera italiana (USI), CH-6605 Locarno, Switzerland

ARTICLE INFO

Keywords:
Solar radio burst
Frequency drift rate
Shock speed
Electron velocity
Type II and type III bursts
CALLISTO

ABSTRACT

Solar radio bursts are sudden peaks in the low-frequency radio emissions originating from the sun. These emissions, while revealing important insights into underlying physical mechanisms in solar physics, can also help predict space weather events that could have adverse effects on satellite communications and the global energy grid. A thorough understanding of this phenomena demands the collection and analysis of solar emission data over vast geographical and time scales. In this regard, the e-CALLISTO network plays a major role through having already archived more than 20 years worth of solar radio burst data. Leveraging on the advances in data analysis techniques, this data can be used to review the statistical significance of burst properties of type II and type III solar radio bursts and hence more importantly the magnetic field measurements of the active regions. In order to process the e-CALLISTO data, a software containing several data reduction processes is introduced to optimize the data analysis via a graphical user interface (GUI). The program is capable of reading out data from any CALLISTO receiving station, while offering visualization capabilities such as the color-corrected spectrum view, the plot of frequencies of the highest intensity, the individual frequency spectrum, the solar burst isolation portal, the fitting model for the radio burst, and the drift rate curve of the burst. These are achieved through using the raw "fits" files of spectra to perform background RFI reduction, identify and isolate solar radio burst regions, model the peak frequency variation using curve fitting, and thereby determine the frequency drift rates. The method can be directly applied to Type II and III solar bursts while providing space for tailoring and modification. In this work, the slow drift type II radio bursts were fitted by exponential decay and the fast drift type III radio bursts were approximated as linear decay. Hence, the frequency drift rates were computed for type II and type III radio bursts. The application is used to analyze several Type II and Type III solar radio bursts and depending on the bust type shock speed and electron velocity were determined. The GUI interface eliminates the time-consuming subjective manual analysis of e-CALLISTO data thereby making the analysis of solar radio bursts a routine and rapid process.

1. Introduction

The frequency range of radio bursts emanating from the sun's surface can spread over 20 KHz to 1 GHz (decameters to centimeters in wavelength) (Benz et al., 2009). The band of radio waves at the length scale of meters and decimeters can be used as a diagnostic of the solar process (McLean and Labrum, 1985; Benz et al., 2004). This wavelength regime is produced at the source location of radio bursts from the corona to the far corona and solar wind. The course of solar radio bursts (hereafter SRBs) can be explained with different emission processes (Uchida, 1960; Behlke, 2001) but in general the energy release of the bursts is associated with the magnetic energy in active regions. The shock waves, and electron beams escaping from open field lines are common emission processes of SRBs. The spectrum of SRBs is an arrangement of frequency space that varies with time. As observations claim, most of the solar bursts are observed below the 400 MHz frequency level. These SRBs could be categorized into five main types (Monstein, 2011).

1. Type I burst (Noise storm)
2. Type II burst (Slow drift rate)
3. Type III (Fast drift rate)
4. Type IV burst

* Corresponding author.
E-mail address: yets19971007@gmail.com (Y. Hettiarachchi).

https://doi.org/10.1016/j.newast.2024.102194
Received 5 September 2023; Received in revised form 17 January 2024; Accepted 19 January 2024
Available online 26 January 2024

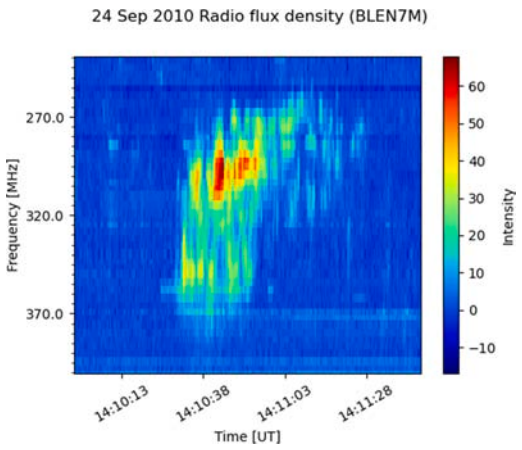

Fig. 1. The radio flux density spectrum of a Type I SRB observed at Bleien observatory, Switzerland on 24th of September 2010 between 14:10 and 14:11.

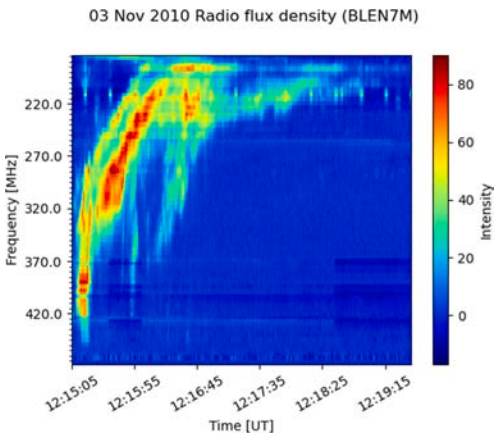

Fig. 2. The radio flux density spectrum of a Type II solar radio burst with "harmonics" and "herringbones" observed at Bleien, Switzerland on 3rd of November 2010 between 12:15 and 12:19.

5. Type V burst

1.1. Type I burst (noise storm)

Type I storm is commonly known as "Noise Storm" which consists of a long series of short solar bursts continuing over hours or even as long as a few days (Fig. 1). The polarization of these bursts is always circular, but it could change within a day. This could occur in the background of a large number of overlapping bursts, thereby giving the appearance of a continuum. Noise storms are generally spread over a large frequency band which is just under 350 MHz (Monstein, 2011).

1.2. Type II burst (slow drift rate)

Type II bursts have a low drifting rate. A slow drift burst could appear as a narrow band of intense radiation that drifts gradually or sometimes irregularly through and towards lower frequencies (Fig. 2). The type II SRBs results from plasma emissions generated by shock waves (Cane and Stone, 1984). Even though this type of burst shows the presence of a second harmonic, very often it shows some characteristics of "Herring Bones". Herring Bones refer to the bursts which are plasma radiation resulting from Langmuir waves generated by energetic electron stream accelerated at the type II bursts (Cane and Stone, 1984; Cairns and Robinson, 1987). The characteristic velocity of the solar disturbance which gives rise to these slow bursts may be deduced from their rate of change of frequency. This velocity is of the order of 1000 $\mathrm{km\ s^{-1}}$ (White, 2007; Benz, 2009). The presence of corona mass ejections (CMEs) and type II SRBs has become highly correlated that the shock that produce type II burst are being driven by CMEs (White, 2007; Gopalswamy et al., 2005). These waves are propagated outward at some small multiple of the thermal velocity of the protons, would also be traveling at a velocity of the order of 1000 $\mathrm{kms^{-1}}$ (Moreton, 1960; Warmuth, 2015).

1.3. Type III (fast drift)

Type III SRBs are the most common type of emissions in solar energetic events (Benz et al., 2009; Benz, 2009). This type of burst has a high drift rate, typically in the order of 100 $\mathrm{MHz\ s^{-1}}$ (Behlke, 2001). Type III is a more common phenomenon that drifts rapidly toward low frequencies within a few seconds (Fig. 3). These bursts typically occur in groups of 3 to 10 with a total duration of about 60 s. Type III SRBs reflect the following characteristics of the radio burst phenomenon. They occur over the frequency range of 10 kHz to 10 GHz (Fainberg and Stone, 1974). Type III SRBs are generated

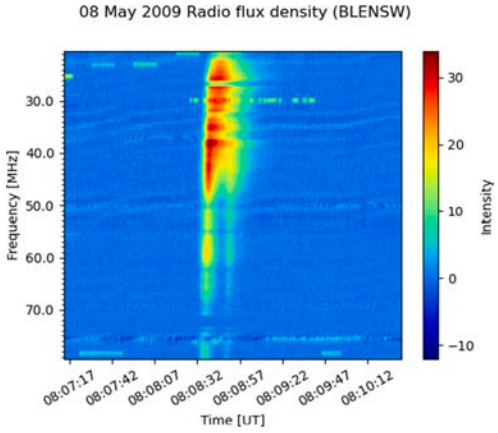

Fig. 3. The radio flux density spectrum of a low frequency, isolated Type III SRB observed at Bleien, Switzerland on 8th of May 2009 between 08:07 and 08:10.

by the streams of fast electrons in the corona (Zaitsev et al., 1972). Generally, type III bursts could be subdivided into type IIId and type IIIb bursts (Behlke, 2001). Type IIId bursts drift faster than normal type III bursts and arise from the relativistic head of the electron beam (Poquerusse, 1994). The IIIb bursts are chains of split-pair and narrow band bursts which may be seen only in high-resolution spectra. Type III bursts have been extensively classified by Wild and McCready (1950).

1.4. Type IV

In this type of burst, continuum radiation is a steady enhancement of the background level over a wide bandwidth of the spectrum, and it could be observed often associated with noise storms (type I). Type IV bursts can be found frequently over the band of more than 300 MHz and it often occurs after great outbursts. The time duration of a type IV burst can vary from 10 min to 300 min. Type IV bursts could be seen in wavy, periodic intensity variation in the frequency spectrum (Monstein, 2011) as seen in Fig. 4.

1.5. Type V

Type V radio bursts are almost always associated with type III radio bursts and follow them just after a few seconds. They have an indicator flag pointing to higher frequencies in front of the radio burst. Therefore, they could be identified easily. This emission has a bandwidth of less

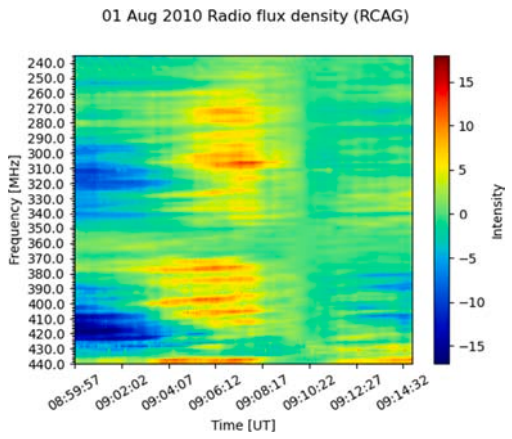

Fig. 4. The radio flux density spectrum of Type IV SRB observed in Badary, Russia on 01st of August 2010 between 08:59 and 09:14.

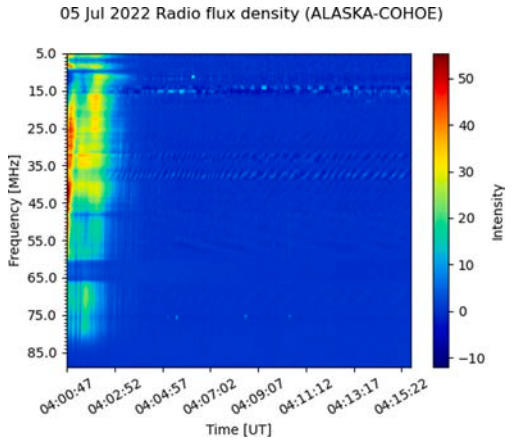

Fig. 5. The radio flux density spectrum of Type V radio SRB observed at COHOE, Alaska on 05th of July between 4:00 and 4:15.

than 200 MHz and the duration is mostly less than 1 min (Monstein, 2011). The emission mechanism of this type would be plasma mode transformation and the exciter is electron streams (Fig. 5).

1.6. The e-CALLISTO network

The parameters of different types of SRBs are used to characterize corona mass ejections (CMEs), solar flares and space weather. The data produced by the ground-based and space-based arrays and missions are readily available to investigate solar phenomena. e-CALLISTO global network (Benz et al., 2009) is a dedicated program for the observation of solar activity in radio bands and archiving data from 1978. The frequency coverage of this spectrometer is between 45 MHz and 870 MHz with a frequency resolution of 62.5 kHz over 200 channels. The spectrograms present all channels versus time in graphical form covering 15 min of observation (Benz et al., 2009). The database consists of spectrograms of the sun during relatively calm periods as well as during periods of disturbance. Hence, spectrograms with radio bursts should be separated from the blank spectrograms. This process was solved by Mario et al. (2022) in their application of automatic detection of e-CALLISTO solar radio bursts using deep neural networks. Although a number of data analysis tools are available to analyze e-CALLISTO spectrometer data (Monstein et al., 2023), yet a small fraction of data has been analyzed for scientific purposes. To find the properties of exciter of SRBs, pre-processing is needed to remove background noise commonly known as Radio Frequency Interference (RFI). In general, the SRBs are circular polarized (Morosan et al., 2022). Except for few CALLISTO receiving stations, most of the stations consist of Log-Periodic dipole antenna which observes in plane polarization. Therefore, the observed spectra sometimes show non-continued flux over the time. Fig. 16 shows such a discontinuity effect in the type II SRB. The low resolution of the image spectra is another effect to compensate in the pre-processing stage. These initial corrections should be able to do at a single stretch and thereafter determine the necessary parameters of SRB.

This application is developed to analyze SRB data obtained from the e-CALLISTO program which were taken from 73 active stations[1] around the world. We introduced a GUI application to reduce the time spent on initial data reduction steps and to determine the frequency drift rates of the CALLISTO data. The facility provides a layout to utilize more data from the e-CALLISTO archive and hence intended to increase parameter statistics of the solar activity. In Section 2, the objectives of the project are listed, while in Section 3 the detailed procedure of the function of the GUI is laid out. The usage of the application is explained in detail with the results of type II and type III SRBs in Section 4. The constraints, further enhancements, and conclusions of the application are discussed in Section 5.

2. Objectives

2.1. Development of an easy-to-use method to analyze type II and type III SRBs

There are different techniques developed to analyze CALLISTO solar radio spectra with a set of supporting software tools available at e-CALLISTO.[2] Image processing methods and the extraction of data from spectra were introduced in these techniques and software tools. However, a fully automated process of data handling is yet to be done and this effort has been to develop a tool for image processing, enhancing, cropping, and finally extracting the frequency drift rates through a curve fitting in a semi-automated system. This application is timely and important to analyze the giga bytes of CALLISTO data. Therefore, this tool provides an effective, efficient, and versatile method to analyze SRBs.

2.2. RFI reduction of the spectra and isolation of the burst

Radio observations are not affected by poor weather conditions. Nevertheless, the radio frequency interference (RFI) of numerous sources are imprinted on the radio spectrum and merged with the SRB (Fig. 6). These RFIs are troublesome as they are produced by sources ranging from nearby electronics to satellites in the very broadband frequency range which overlaps with the CALLISTO observation range (Monstein et al., 2006). The common approach to remove the RFI is subtracting the source image spectrum using a blank image spectrum taken by the same station within the observation range of the radio burst. Gordo et al. (2023) used subtraction of the average spectrum over time in their automatic burst detection algorithm. Guo et al. (2022) reduced the influence of RFI on the spectrum image, using the channel normalization method to enhance the dynamic spectra feature recognition from the instrument noise. However, most of these methods are used in automatic detection of radio bursts rather than the calculation of drift rate using frequency distribution over time. The methods mentioned above are applied to the whole dynamic spectra so that the intensity of the actual SRB is modified. Therefore, the objective of obtaining the frequency drift rate by curve fitting may be affected by these methods. We propose a method of isolating the burst and reducing the background RFI through an optimization process. This method is discussed in Section 3.

[1] https://www.e-callisto.org/

[2] https://www.e-callisto.org/Software/Callisto-Software.html

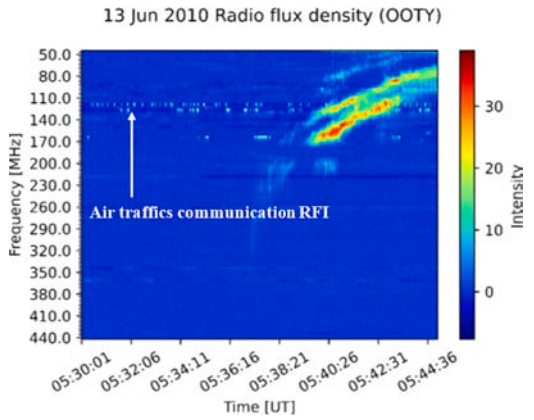

Fig. 6. The dynamic radio flux density spectrum of a Type II solar radio burst, interrupted by air traffics communication RFI. The 1st harmonic of the fundamental radiation is also present.

2.3. Calculating the frequency drift rates of the SRBs

Due to the complexity of the burst distribution in the spectra, in general, the mean drift rate was taken considering the initial and final status of the burst. This average drift rate does not perfectly represent the non-linear drifts like type II bursts. Further, there should be a method to determine the drift rate at any frequency within which the burst occurs. For this purpose, a best-fit model that can represent the burst is determined over the frequency range. Using the best-fitted model, the first derivative of the function is taken as the frequency drift rate. The project was done in Python (Anaconda Navigator-Spyder 5.0). The data files were downloaded through the e-CALLISTO website as "fits" files. The user inputs are taken through a graphical user interface (GUI).

3. Methodology - Graphical user interface and frequency drift analysis

The entire code can be implemented through an easy-to-use Graphical User Interface (GUI). The program allows for the Flexible Image Transport System (fits) files of e-CALLISTO data to be imported from a local drive. Initially the GUI visualize the raw image with the color intensity to differentiate the distribution of the SRB over the background noise. All CALLISTO receivers are identical with 200 channels in frequency (y-axis) and 3600 channels in time (x-axis). The 200 channels are calibrated to the frequency range defined by the observation stations. For example, In Sri Lankan station, we observe the SRBs in the frequency range of 45 MHz to 85 MHz. Therefore, this range is represented by 200 channels. Thus, the calibration scale differs from station to station. In this application, the burst is isolated from the common grid of channels 200 × 3600, and as a result the frequency and time axes are modified and new frequency and time ranges are assigned. However, The time axis of all the spectra of e-CALLISTO archive represents 15 min by 3600 channels, each channel is 0.25 s. Since time calibration is identical for all the stations we directly used the number of channels in the time axis for the isolation process of the SRBs. The IMG1 option in GUI (Fig. 7) visualizes the raw spectrum and IMG2 option enhance and re-scale the color map in order to contrast the burst from the background which creates an clear image for identifying the burst's time range and frequency range for isolation. Thereafter, the intensity of the input frequency channel (1 to 200) will be plotted along the time axis for a better understanding of the burst area for the isolation. This option is given to visualize the intensity distribution of each frequency channel along the time axis through a graphical plot using IMG3. The rest of the GUI functionalities will be discussed with

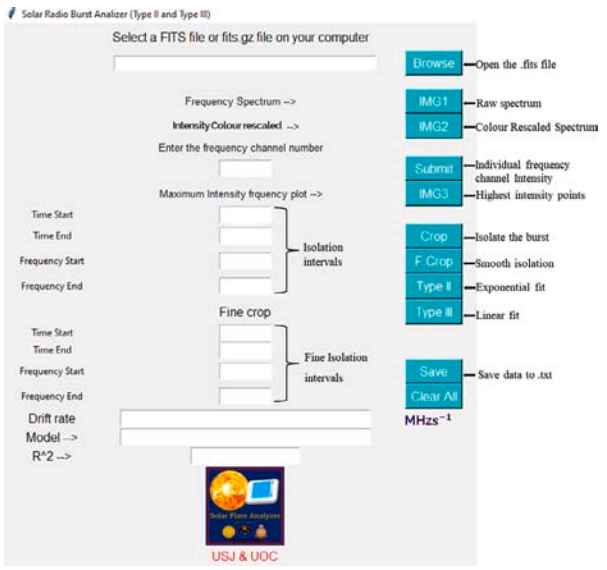

Fig. 7. The Graphical User Interface of the "Solar Radio Burst Analyzer — type II and type III. The executable (.exe) file of the GUI is available at https://github.com/YetsVihanga/Callisto-SRB-analyzer.git.

the examples in Sections 3.1 and 3.2. The program was named Solar Radio Burst Analyzer (type II and type III). This GUI was created with Tkinter Python module. The interface was written with latest python version thus, this GUI interface is mostly recommended for ×64 bits versions of Windows 7 and above. This program is also compatible with Linux. For users who prefer any operating system other than Microsoft Windows, the python script can be downloaded from the website, "Git-hub".[3] The following features were added in the GUI (Fig. 7).

1. Intensity graphs of individual frequency channels (IMG3)
2. Crop and Fine Crop for isolating the radio burst at a smoother scale (Crop and F Crop)
3. Display of the fitted model (Type II and Type III)
4. Extract frequency drift rates and Goodness of fit (R^2)

3.1. Analyzing type III: Fast drift rate SRBs

The type III burst observed by Australia-ASSA on 25th of September 2021 (Fig. 8) was analyzed using the Intensity Matrix in the GUI application. In this method, burst isolation is done without applying any image subtraction to the burst spectrum. Therefore, the raw spectrum in Fig. 8 preserves its originality. In the Intensity Matrix Method, the spectrum is converted to an intensity matrix. The matrix consists of solar radio flux in the z, time in the x, and frequency in the y directions. The analysis and calculations were done with raw data, where the qualitative properties of the spectrum are preserved. Initially, each frequency channel (from 1 to 200) was scanned along the time axis and the time stamp of the highest intensity points was recorded. This can be visualized through the submission of frequency channel (1–200) in GUI. The IMG3 option provides the highest intensity points along the time axis as a scatter plot shown in Fig. 9. This visualization is important to decide the isolation area of the burst from the rest of the image.

Thereafter the burst can be disentangled from the rest of the signals by defining the time and the frequency limits of the burst range. Isolation of the SRB was done with matrix and vector calculation methods in Python. The plot of Fig. 9 can be used to define the x coordinates and y coordinates where the burst is located (see Fig. 10). After defining

[3] https://github.com/YetsVihanga/Callisto-SRB- analyzer.git

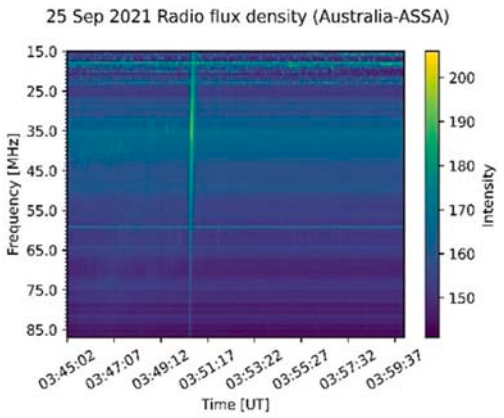

Fig. 8. A Radio flux density spectrum of type III SRB generated by "The solar radio burst analyzer — type II and type III". This is type III SRB captured by Australia-ASSA on 25th of September 2021.

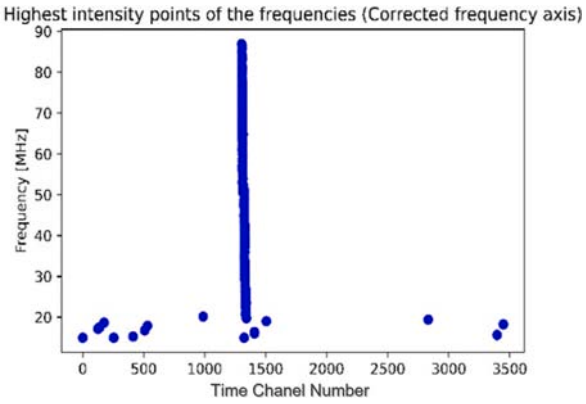

Fig. 9. The scatter plot of the highest intensity points of each frequency channel of the burst in Fig. 8. This plot is obtained using the IMG3 option of the GUI. The y-axis is flipped and the x-axis is given in time channel numbers where 1 channel represents 0.25 s.

the intervals of time and frequency ranges for the isolation, the values beyond the ranges were assigned 0 in the intensity matrix as shown in Fig. 11. The isolation boundaries (both time and frequency) of the burst were fed to GUI through isolation intervals (Fig. 7). The Crop command in GUI will execute the isolation and display the cropped SRB as shown in Fig. 12. This figure represents the type III SRB shown in Fig. 8. Note that the total channel numbers in time axis are now reduced to 35 which equals to 8.75 s.

The isolated radio burst is subjected to the drift rate analysis through curve fitting. Due to the fast drift nature of type III bursts the drift rate could be modeled with linear fit (Wijesekera et al., 2018). Hence for type III, a linear model is suggested to compute the drift rates. The drift rate is equal to the slope of the modeled Eq. (1).

$$f = \frac{df}{dt}t + c \tag{1}$$

where, f = frequency, t = time, $\frac{df}{dt}$ = drift rate

3.2. Analyzing type II: Slow drift rate SRBs

A similar approach was followed for the isolation of type II bursts as mentioned in Section 3.1. Fig. 13 is the radio flux density spectrum of a type II radio burst observed at OOTY, India on 13th of June 2010. Fig. 14 shows corresponding distribution of highest intensity points of the burst. The inbox of Fig. 14 indicates that there are several high-intensity points of frequency along the same time line. These points

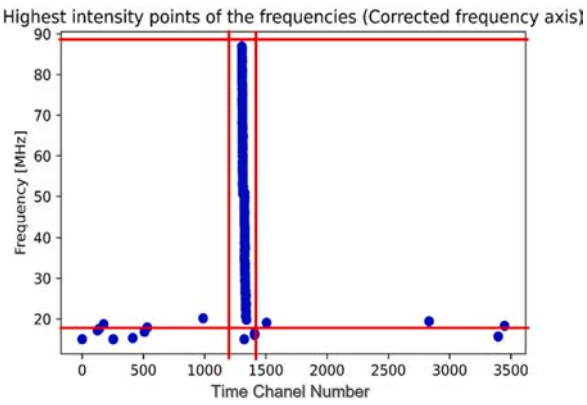

Fig. 10. Defining the time and frequency intervals for the isolation process of the radio burst with the GUI; "Crop" option.

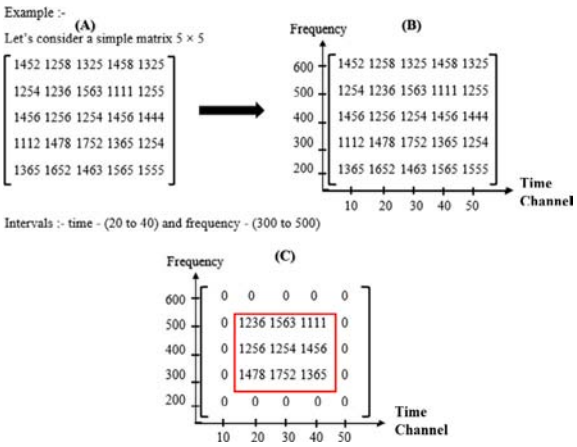

Fig. 11. Intensity matrix method: The radio flux density spectrum of SRB can be represented by a matrix with the intensity values with respect to the time channel number and frequency. The panel A shows a part of (5 × 5) entire intensity matrix with the original intensity values. Panel B is the entire grid. Panel C shows the cropped intensity matrix. The rest of the intensities of the grid were brought to zero after cropped area (red box) is identified.

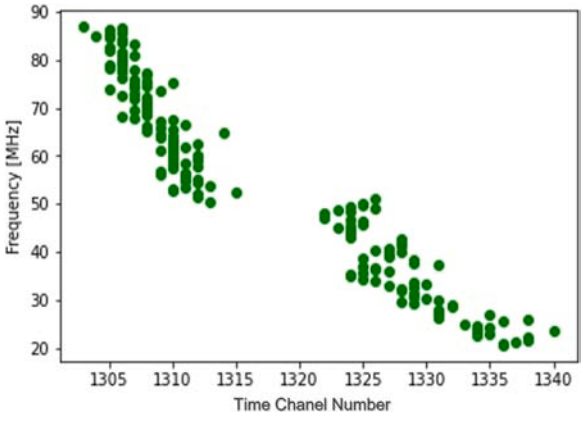

Fig. 12. The scatterplot of the intensity distribution of the type III SRB which was cropped in Fig. 9. Note that the time axis is modified.

were generated by an instrumental effect. The average intensity was taken for these multiple y values of the same time channel. Thereby redefining the intensity distribution of the type II burst for the model fitting (see Fig. 14). For all type II bursts, a non-linear least squares method was used as the model fitting technique. To increase the

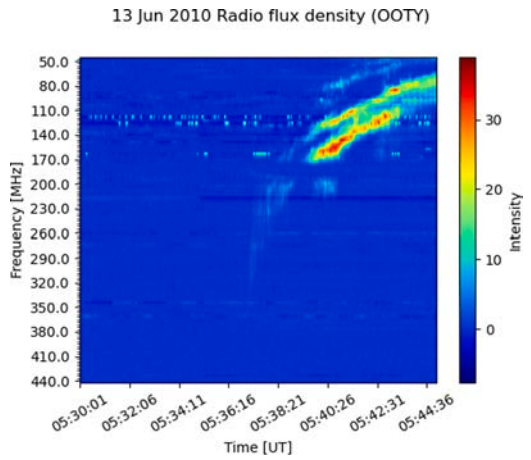

Fig. 13. The Frequency intensity spectrum of a type II SRB (OOTY) 13th June 2010.

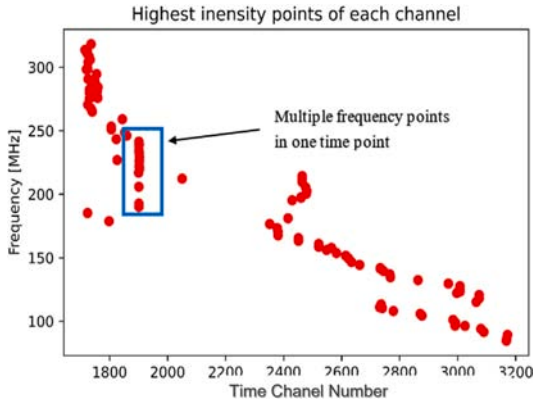

Fig. 14. The plot of highest intensity points of type II burst. The inbox shows multiple frequency points occur for a same time channel.

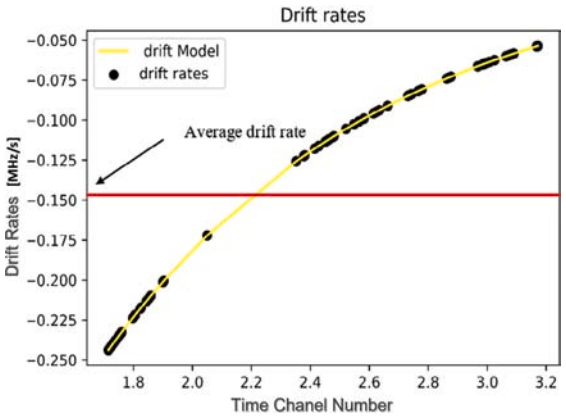

Fig. 15. Drift rates obtained from the curve fitting to the type II SRB in Fig. 13. The black dots represent the drift rates of the data points of the highest intensities recorded in Fig. 14 and the red horizontal line is the average value of all the drift rates in black dots.

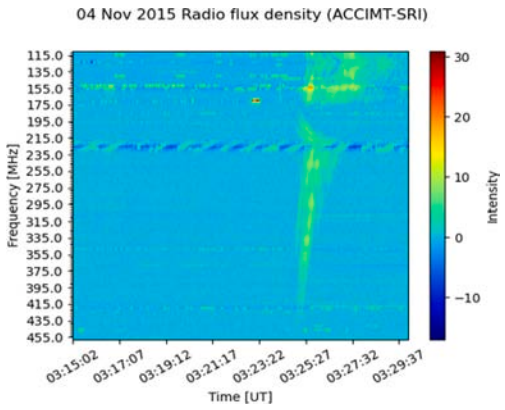

Fig. 16. Raw image of the spectrum taken from Sri Lanka CALLISTO station on 4th November 2015. This is a type II burst.

accuracy, the number of steps for the least square method was increased from its initial number of 1500 up to 5000 steps. In this method, p the model function is defined with unknown parameters β, $y = p(x, \beta_1, \beta_2, \ldots)$ and the error of the modeled fit and the actual data was minimized by changing the parameter values. The sum of the square of errors is defined as; $\Sigma_{i=1}^{n}(p(x, \beta_i) - y_i)^2$. If the y_i data points have the corresponding errors on them, then minimizing $\Sigma_{i=1}^{n}(p(x, \beta_i) - y_i)^2/\sigma_i^2$ gives the maximum-likelihood estimate for β_i (Chakrabarty, 2014). The frequency drift in type II SRBs is proportional to the rate of change in electron density (dN/dr) in the solar corona (Newkirk, 1961, 1967). As a result the fitting function could be taken as an exponential function for type II bursts (Wijesekera et al., 2018). Therefore, the suggested exponential model is,

$$f = ae^{-\frac{(b+t)}{t}} + c \tag{2}$$

where, f = frequency, a, b, c are function parameters t = time

After the proper modeling of the fit for the type II burst, it is possible to obtain the drift rate at any point in the time span of the burst. This is an advantage of our method of curve fitting. For the calculation of shock speed, the frequency drift rate is an essential parameter. Therefore, the frequency drift rate should be determined for a SRB. For non-linear fittings, the drift rate changes over time and there are no specific rules to read out the drift rate for a particular burst. In general, the drift rate at the beginning or at the end of the burst can be read out but this is not a suitable method because at the start point or at the end point of the curve, it is not possible to determine the slope of the curve accurately. Therefore, the derivative (df/dt) of the fitted function was plotted over time, and the average value was taken as the drift rate of the solar radio bust as shown in Fig. 15. The GUI provides this average drift rate at the end of the application. If user wants drift rate at a specific frequency that can be obtained from the text file which we provide data of the fitting function.

4. Application and results

Fig. 16 shows a type II SRB observed at the Sri Lanka CALLISTO station (ACCIMT- SRI-20151104-031502-F) on 04th November 2015. The radio burst is recorded between 03:23 UT and 03:27 UT with a duration of 4 min. This raw file is subjected to the procedure mentioned in Section 3 and resulted in a reasonably good exponential fit as shown in Fig. 17. For the optimization of the curve fitting, the data points can be deleted interactively to eliminate the outliers and reduce the mean square value (R^2) of the fit given in the GUI. In principle, the radio bursts start at a higher frequency and end up with a lower value. The distribution of frequency drift rate is separately shown in Fig. 18. However, for the computation of shock speed or electron velocity given in Eq. (4), a drift rate should be defined for the burst. Therefore, we used the averaged value of the drift rates. This value is given in Table 1 under the 04/11/2015, Sri Lanka.

Fig. 19 is a type III SRB observed at the Greenland station (Greenland-20210218-17 5352-62) on the 18th February 2021. The drift is fast and recorded in 1 min between 18:04 UT and 18:05 UT. The burst is approximated by a linear model (Fig. 20) and the drift rate is

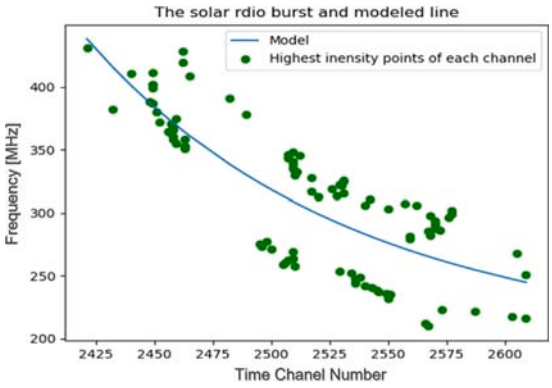

Fig. 17. Generated scatter-plot of the highest intensity points and its model fit of the type II burst observed at ACCIMT-Sri Lanka-20151104-031502-F. The best fit was obtained using Eq. (2).

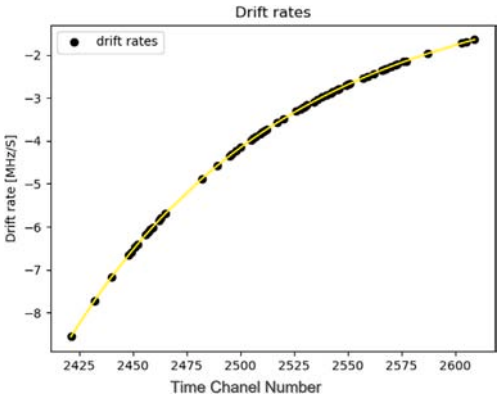

Fig. 18. The calculated drift rates using the non-linear model fit shown in Fig. 17 for the type II burst: ACCIMT-Sri Lanka-20151104-031502-F. The average of all drift rates in black dots was taken as the drift rate for the SRB. The value is given in Table 1 under 04/11/2015, Sri Lanka.

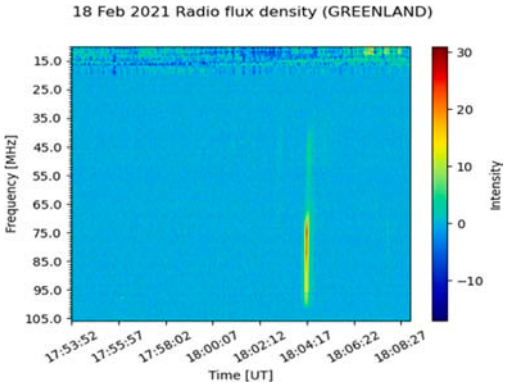

Fig. 19. The radio flux density raw spectrum of type III SRB.
Source: GREENLAND-20210218-17 5352-62.

given in Table 1 under 18/02/2021, Greenland. Similarly, several type II and type III radio bursts were analyzed for drift rates and tabulated in Table 1. The drift rates in Table 1 were used to calculate the shock speeds or electron velocities as mentioned in Table 2.

5. Discussion

This is high time to introduce a fully automated AI-based system to classify and analyze the SRBs vastly observed by the e-CALLISTO network. Bussons Gordo et al. (2023) has introduced a deep learning approach only to detect the radio burst from ground-based and space-based archives. Scully et al. (2021) introduced a classification of type III radio burst through deep learning in real-time. The determination of frequency drift rates is an essential parameter that leads to determining the properties like shock speed, electron velocity, electron density, and magnetic fields of SRBs (Shanmugaraju et al., 2005). Due to the very complex and noisy nature of the radio burst spectra, the analysis procedure is time-consuming and inconsistent. Though this application is not fully autonomous, this GUI-based interface reduced time consumption by introducing important options for the user such as isolation of the burst from the RFI, curve fitting, and drift rate estimation in one stretch. Therefore, this option provides analysis of large data sets to find the statistical significance of properties of type II and type III SRBs. The frequency change per unit time is generally accepted as the drift rate

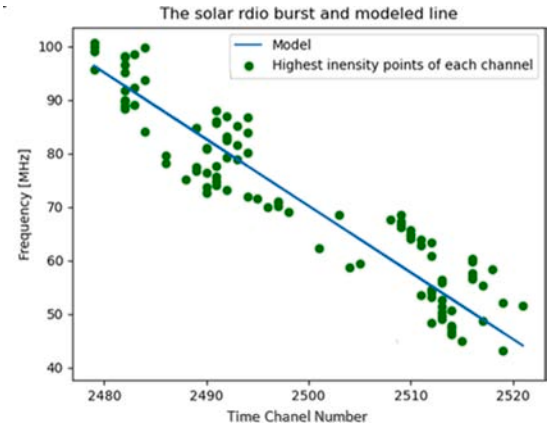

Fig. 20. The highest intensity points and the fitted model of the isolated type III SRB observed at Greenland (Fig. 19).

Table 1
The tabular of average frequency drift rates of analyzed Type II and Type III solar radio bursts.

Burst Type	Date	Station	Drift Rate MHz/s
Type II	04/11/2015	Sri Lanka	−3.8652
	04/11/2015	Kazakhstan	−3.7124
	04/11/2015	India (GAURI)	−3.4636
	04/11/2015	India (OOTY)	−3.4936
	16/04/2014	Roswell	−1.7572
	16/04/2014	Roswell	−0.1044
	09/10/2021	Kazakhstan	−0.2044
	09/10/2021	Australia (ASSA)	−0.1585
	09/10/2021	Austria (UNIGRAZ)	−0.1960
	09/10/2021	Indonesia	−0.2048
	09/10/2021	Sri Lanka	−0.1561
Type III	08/03/2020	USA (ALASKA)	−4.5756
	19/11/2013	Switzerland (BLEN7M)	−9.8156
	18/02/2021	Greenland	−4.9840
	16/12/2021	Austria (UNIGRAZ)	−13.3361
	16/12/2021	BIR	−10.9312
	16/12/2021	Denmark	−15.9517
	16/12/2021	Triest	−12.4205
	16/12/2021	Swiss (Landschlacht)	−11.5388
	16/12/2021	Spain (Peralejos)	−11.6836

Table 2
The tabular of velocities of Type II and Type III SRBs. The velocity represents the shock speed for type II bursts and electron velocity for type III bursts.

Burst Type	Date	Station	Velocity ms^{-1} (10^6)
Type II	04/11/2015	Sri Lanka	3.7749
	04/11/2015	Kazakhstan	3.6256
	04/11/2015	India (GAURI)	3.3826
	04/11/2015	India (OOTY)	3.4119
	16/04/2014	Roswell	1.7161
	16/04/2014	Roswell	0.1019
	09/10/2021	Kazakhstan	0.1996
	09/10/2021	Australia (ASSA)	0.1547
	09/10/2021	Austria (UNIGRAZ)	0.1914
	09/10/2021	Indonesia	0.2000
	09/10/2021	Sri Lanka	0.1524
Type III	08/03/2020	USA (ALASKA)	60.650
	19/11/2013	Switzerland (BLEN7M)	130.10
	18/02/2021	Greenland	66.064
	16/12/2021	Austria (UNIGRAZ)	176.77
	16/12/2021	BIR	144.89
	16/12/2021	Denmark	211.44
	16/12/2021	Triest	164.63
	16/12/2021	Swiss (Landschlacht)	152.94
	16/12/2021	Spain (Peralejos)	154.86

of a SRB. The general definition is given in Eq. (3).

$$\text{Drift rate} = \frac{df}{dt} = \frac{(f_e - f_s)}{(t_e - t_s)} \tag{3}$$

where, f_e = End frequency, f_s = Start frequency, t_e = End time, t_s = Start time

According to Shanmugaraju et al. (2009), the drift rate can be defined as mean drift rate and relative drift rate. Generally, the drift rate of a radio burst is taken as the mean drift rate by taking the initial and final conditions only. Since we do a curve fitting, for the radio burst, the drift rate can be determined at any point of the burst. However, for type III burst, the linear approximation provides a single value for the drift rate while for the type II burst its the first derivative of the curve. This flexibility is more generalized the use of drift rates for parameter calculations. We included the velocities calculated by Eq. (4) for few case studies of type II and type III bursts. Newkirk uniform electron density model (Newkirk, 1961) of solar corona is used in Eq. (4).

$$V = \frac{(2\frac{df}{dt})N}{(f\frac{dN}{dr})} \tag{4}$$

where, N - electron density, f - plasma frequency, $\frac{dN}{dr}$ - change of N with respect to height

In summary, the method, which was developed in this work, provides a mechanism where the recorded SRBs of the CALLISTO files can be directly used as input to determine the solar burst pattern, frequency drift rate and shock or electron velocity. To check the consistency of the application, several type II and type III bursts simultaneously observed by different stations were analyzed. The shock speeds calculated for the type II burst recorded on 04/11/2015 at four stations (Table 2) are consistent with 90% with the average value. As the fundamental physics behind the eruption of a SRB and its subsequent propagation through space and the Earth's upper atmosphere is still being debated, it is difficult to place a degree of certainty in the accuracy of the mathematical modeling. Hence, scientists rely on statistical methods to ascertain the degree of conformity of a given model to a data set. Ideally, the development of a computational technique requires the output of the method to be compared with established data to validate the new method. Although SRB analysis has been done in case-by-case at a greater depth, a bulk analysis could not be performed due to the lack of a standardized method of computation in the past. This leads to the difficulty of obtaining a statistical significance of the success of a model. We hope to use the facility for mass scale analysis and results will be published in our forthcoming paper.

6. Conclusion

The frequency drift rate is a key parameter to determine the characteristics of type II and type III SRBs. The exact relation of CMEs, flares and type II bursts is still uncertain. To make better conclusions of these energetic events, more data has to be analyzed and improve the statistics of the parameters. However, this area of study has been plagued by the lack of a standardized method of analysis. We introduced dynamic spectral image processing routine with a GUI. The method is based on intensity matrix which includes RFI elimination, burst isolation and curve fitting. The routine can determine frequency drift rate for any type II and type III radio bursts at one stretch. Therefore, application fulfills the underutilized SRB data archived at e-CALLISTO network. Using the tool, several bursts were analyzed determining their drift rates and exciter velocities. We modeled the type II bursts with an exponential function and type III with a linear fit. Therefore, the application should be used with care because of the chaotic behaviors of the SRBs. Use of application for large scale analysis of SRBs is desired to enhance the performance.

CRediT authorship contribution statement

Yashan Hettiarachchi: Writing – review & editing, Writing – original draft, Visualization, Software, Project administration, Methodology, Investigation, Formal analysis, Data curation, Conceptualization. **Janaka Adassuriya:** Writing – review & editing, Writing – original draft, Validation, Supervision, Resources, Project administration, Methodology, Formal analysis, Data curation, Conceptualization. **Chandana Jayaratne:** Writing – review & editing, Validation, Supervision, Project administration, Investigation, Conceptualization. **Sasani Jayawardhana:** Writing – review & editing, Writing – original draft, Validation, Supervision, Project administration, Methodology, Investigation, Formal analysis, Conceptualization. **Christian Monstein:** Writing – review & editing, Validation, Supervision, Resources, Project administration, Investigation, Data curation, Conceptualization.

Declaration of competing interest

The authors declare that they have no known competing financial interests or personal relationships that could have appeared to influence the work reported in this paper.

Data availability

Data will be made available on request.

References

Behlke, R., 2001. Solar radio bursts and low frequency radio emissions from space. IRF Scientific Report 275.

Benz, A.O., 2009. 4.1. 2.8 Radio bursts of the non-thermal sun. In: Solar System. Landolt-Börnstein-Group VI Astronomy and Astrophysics, Vol. 4. Springer, pp. 189–203.

Benz, A.O., Monstein, C., Meyer, H., 2004. CALLISTO-A new concept for solar radio. arXiv preprint astro-ph/0410437.

Benz, A., Monstein, C., Meyer, H., Manoharan, P., Ramesh, R., Altyntsev, A., Lara, A., Paez, J., Cho, K.-S., 2009. A world-wide net of solar radio spectrometers: E-CALLISTO. Earth Moon Planets 104 (1), 277–285.

Bussons Gordo, J., Fernández Ruiz, M., Prieto Mateo, M., Alvarado Díaz, J., Chávez de la O, F., Ignacio Hidalgo, J., Monstein, C., 2023. Automatic burst detection in solar radio spectrograms using deep learning: DeARCE method. Sol. Phys. 298 (6), 82.

Cairns, I.H., Robinson, R.D., 1987. Herringbone bursts associated with type II solar radio emission. Sol. Phys. 111 (2), 365–383.

Cane, H.V., Stone, R.G., 1984. Type II solar radio bursts, interplanetary shocks, and energetic particle events. Astrophys. J. (ISSN: 0004-637X) 282, 339–344, Part 1. Previously announced in STAR as N83-17435.

Chakrabarty, D., 2014. Curve fitting: Step-wise least squares method. Aryabhatta J. Math. Inform. 6 (1), 15–25.

Fainberg, J., Stone, R.G., 1974. Satellite observations of type III solar radio bursts at low frequencies. Space Sci. Rev. 16 (1–2), 145–188.

Gopalswamy, N., Aguilar-Rodriguez, E., Yashiro, S., Nunes, S., Kaiser, M., Howard, R., 2005. Type II radio bursts and energetic solar eruptions. J. Geophys. Res. Space Phys. 110 (A12).

Gordo, J.B., Ruiz, M.F., Mateo, M.P., Díaz, J.A., Hidalgo, J.I., Monstein, C., et al., 2023. Automatic burst detection in solar radio spectrograms using deep learning: Dearce method.

Guo, J.-C., Yan, F.-B., Wan, G., Hu, X.-J., Wang, S., 2022. A deep learning method for the recognition of solar radio burst spectrum. PeerJ Comput. Sci. 8, e855.

Mario, F.R., Javier, B.G., Manuel, P.M., Christian, M., 2022. Automatic detection of e-Callisto solar radio bursts by Deep Neural Networks. In: 2022 3rd URSI Atlantic and Asia Pacific Radio Science Meeting. AT-AP-RASC, IEEE, pp. 1–4.

McLean, D.J., Labrum, N.R., 1985. Solar Radiophysics: Studies of Emission from the Sun at Metre Wavelengths.

Monstein, C., 2011. Catalog of dynamic electromagnetic spectra. Phys. Astron. Electron. Work Bench..

Monstein, C., Csillaghy, A., O. Benz, A., 2023. CALLISTO solar spectrogram FITS files [data set]. International Space Weather Initiative (ISWI). URL http://dx.doi.org/10.48322/pmwd-mk15.

Monstein, C., Manoharan, P.K., Nandagopal, D., 2006. Callisto Spectrum Measurements in Ootacamund. Tech. Rep., ETH Zurich.

Moreton, G.E., 1960. Halpha observations of flare-initiated disturbances with velocities˜ 1000 km/s. Astron. J. 65, 494.

Morosan, D.E., Räsänen, J.E., Kumari, A., Kilpua, E.K.J., Bisi, M.M., Dabrowski, B., Krankowski, A., Magdalenic', J., Mann, G., Rothkaehl, H., Vocks, C., Zucca, P., 2022. Exploring the circular polarisation of low–frequency solar radio bursts with LOFAR. Sol. Phys. 297, 47.

Newkirk, Jr., G., 1961. The solar corona in active regions and the thermal origin of the slowly varying component of solar radio radiation. Astrophys. J. 133, 983.

Newkirk, Jr., G., 1967. Structure of the solar corona. Annu. Rev. Astron. Astrophys. 5 (1), 213–266.

Poquerusse, M., 1994. Relativistic type 3 solar radio bursts. Astron. Astrophys. 286, 611–625.

Scully, J., Flynn, R., Carley, E., Gallagher, P., Daly, M., 2021. Type III solar radio burst detection: A deep learning approach. In: 2021 32nd Irish Signals and Systems Conference. ISSC, IEEE, pp. 1–6.

Shanmugaraju, A., Moon, Y.-J., Cho, K.-S., Kim, Y.-H., Dryer, M., Umapathy, S., 2005. Multiple type II solar radio bursts. Sol. Phys. 232, 87–103.

Shanmugaraju, A., Moon, Y.-J., Vrsnak, B., 2009. Type II radio bursts with high and low starting frequencies. Sol. Phys. 254, 297–310.

Uchida, Y., 1960. On the exciters of type II and type III solar radio bursts. Publ. Astron. Soc. Japan 12, 376.

Warmuth, A., 2015. Large-scale globally propagating coronal waves. Living Rev. Sol. Phys. 12 (1), 1–101.

White, S.M., 2007. Solar radio bursts and space weather. Asian J. Phys. 16, 189–207.

Wijesekera, J.V., Jayaratne, K.P.S.C., Adassuriya, J., 2018. Analysis of type II and type III solar radio bursts. In: Journal of Physics: Conference Series, Vol. 1005. IOP Publishing, 012046.

Wild, J.P., McCready, L.L., 1950. Observatioas of the spectrum of high-intensity solar radiation at meter wavelengths. I. The apparatus and spectral types of solar burst observed. Aust. J. Chem. 3 (3), 387–398.

Zaitsev, V.V., Mityakov, N.A., Rapoport, V.O., 1972. A dynamic theory of type III solar radio bursts. Sol. Phys. 24, 444–456.